Monte Carlo simulations of surface segregation to discover new hydrogen separation membranes

Postma, Jelmer I.; Ferrari, Alberto; Böttger, Amarante J.

DOI
10.1016/j.ijhydene.2022.10.057

Publication date
2023

Document Version
Final published version

Published in
International Journal of Hydrogen Energy

Available online at www.sciencedirect.com

ScienceDirect

journal homepage: www.elsevier.com/locate/he

Monte Carlo simulations of surface segregation to discover new hydrogen separation membranes

Jelmer I. Postma[*], *Alberto Ferrari*, *Amarante J. Böttger*

Materials Science and Engineering, Delft University of Technology, 2628CD Delft, the Netherlands

HIGHLIGHTS

- A computational model to calculate surface segregation is developed.
- Short- and long-range ordering effects in segregation can be predicted.
- The model enables high throughput screening of surface segregation.
- Pd–Cu–Zr is proposed for H_2 separation membranes with reduced poisoning and enhanced H_2 permeability.

ARTICLE INFO

Article history:
Received 12 April 2022
Received in revised form
3 October 2022
Accepted 9 October 2022
Available online 2 November 2022

Keywords:
Monte Carlo
Miedema's model
High throughput
Hydrogen separation
Ternary alloys
Palladium

ABSTRACT

Surface compositions play a predominant role in the efficiency and lifetime of membranes and catalysts. The surface composition can change during operation due to segregation, thus controlling and predicting the surface composition is essential. Computational modelling can aid in predicting alloy stability, along with designing surface alloys and near-surface alloys that can outperform existing materials. In this work, a computational model to predict surface segregation in ternary alloys is developed. The model, based on Miedema's semi-empirical model and Monte Carlo simulations, enables to predict long- and short-range ordering in the surface and subsurface layers. It is used to screen a vast range of alloy compositions to design a novel ternary Pd-based material for H_2 separation membranes. The addition of specific amounts of Cu and Zr to Pd is expected to reduce poisoning and enhance the permeability as compared to pure Pd.

Introduction

The drive towards a hydrogen economy has a great potential to reduce the emission of greenhouse gases, but a number of challenges have to be overcome to make it viable [1]. One of these challenges is the purification of H_2 [2,3]; for instance, high purity (>99.95%) H_2 is needed for general industrial hydrogenation [4] and ultra-pure H_2 (>99.97%) for polymer electrolyte membrane fuel cells [5].

Hydrogen can be purified with metal membranes based on the element Pd, which can efficiently dissociate the H_2 molecule [6–8]. However, membranes made only of Pd have numerous shortcomings, including: i) a phase transition when H is absorbed, which causes embrittlement [9,10]; ii) surface poisoning by CO and H_2S, which decrease the rate at which H can be adsorbed on the surface [11]; iii) high material cost; iv) supply scarcity [12].

Pd-membranes are often alloyed with transition metals to alleviate some of these drawbacks [13,14]. In particular Ag, Au,

* *Corresponding author.*
E-mail address: J.I.Postma-1@tudelft.nl (J.I. Postma).

https://doi.org/10.1016/j.ijhydene.2022.10.057

and Cu have received considerable attention [15–18]: the addition of Ag increases the permeability [18]; the addition of Cu improves the poisoning resistance against H_2S and CO [19,20], but decreases the permeability [21]; the addition of Au improves the poisoning resistance against H_2S and improves the permeability, but Pd–Au membranes are less stable in operation than Pd–Cu membranes, leading to diminishing permeation rates over time [22], and the adsorption of H on Au is endothermic, which is unfavourable for the adsorption of H on Pd–Au membranes [23].

Despite being better than pure Pd-membranes, binary membranes are still sub-optimal and there is ample room for further improvement of their properties by alloying with more elements. In recent years numerous studies have considered Pd-based ternary membranes with a combination of the alloying elements Ag, Au and Cu to combine their advantageous properties in one membrane with varying success. One major challenge of these membranes is controlling the surface segregation [24,25]. Although multicomponent alloys may display novel properties and mechanisms (e.g. unforeseen segregation patterns), they cannot be directly predicted by averaging the properties of unary or binary metals. Therefore, the identification of the right alloying elements and the optimal composition is very difficult, because firstly, several target properties (stability, poisoning, permeability, cost, …) have to be considered simultaneously and secondly, the number of possible compositions to screen to find "sweet spots" increases rapidly when more components are added. For these reasons, standard trial-and-error approaches cannot be employed and simulations are preferred.

Most simulations of surface segregation employ the Langmuir-McLean (LM) equation [26] to compute the layer-by-layer equilibrium composition of each element in an alloy at a given temperature T. The LM equation is a mean-field model that assumes a perfectly random solid solution for each layer and neglects possible ordering within the layers. Although the LM equation works well for ideal solid solutions, it may fail spectacularly when the absolute value of the binding energy between one (or more) pair(s) of atoms is much larger than the typical thermal energy k_BT; in this case, mechanisms such as co-segregation, site-competition, and blocking can arise [27]. Co-segregation describes the effect of two elements segregating to the surface as a result of a low surface energy, of strong binding between the co-segregating elements, or of strong repulsion from one or more elements in the bulk. Site-competition occurs when two elements tend to segregate but one of the two elements has a strong binding with a third element, resulting in the segregation of the other element. Lastly, blocking takes place when one element has a low surface energy but also binds strongly with an element that has a high surface energy. The element with the intermediate surface energy will then segregate. These mechanisms can be more accurately predicted by utilizing Monte Carlo (MC) simulations. These simulations introduce a lattice, thereby lifting the mean-field assumptions of the LM equation. Hence, eventual short-range ordering effects can be predicted.

Several simulation methods have been developed to quantify surface segregation. Density functional theory (DFT) or tight binding Hamiltonians are often used to compute the segregation enthalpies that enter the LM equation, but these methods are computationally too expensive to screen entire ternary phase diagrams for many alloying elements even with the simple LM equation, not to mention for MC simulations. Other models, such as the (modified) embedded atom method (EAM) [28], are more tractable and have been employed in combination with MC. However, reliable potentials are not always available, especially for ternary alloys. An alternative to these methods to compute segregation tendencies are semi-empirical thermodynamic models. Semi-empirical models predict binding and segregation energies based on a database of thermochemical parameters derived directly or indirectly from experiments. The most prominent examples to derive alloy (free) energies in the bulk are Miedema's model [29] and CALculation of PHAse Diagrams (CALPHAD) [30]. In particular, Miedema's model has been successfully employed to predict surface segregation in combination with the LM equation [23,31–34]. Such models are computationally inexpensive and general, since the corresponding databases are very rich and complete especially for transition metals [35], and thus can be used to explore large compositional spaces.

In this work we introduce a computational method based on MC simulations and Miedema's model to predict surface segregation in ternary alloys. We use the thermodynamic model employed in Refs. [23,31–34] to parametrize segregation and interatomic interaction energies. However, we lift the mean-field approximation in those works by performing explicit MC simulations rather than simply using the LM equation. The validity of our model is verified against the available literature for binary and ternary Pd-based alloys. We then couple this model to CALPHAD simulations to screen candidate alloying elements X for novel ternary Pd–Cu–X separation membranes with optimal properties (i.e. high stability, low poisoning, high permeability, and low materials cost). This study finds that the composition $Pd_{48}Cu_{40}Zr_{12}$ optimizes all the required properties and this new material is expected to yield better hydrogen separation membranes than the state-of-the-art. We finally validate our predictions with DFT simulations.

Methods

Monte Carlo simulations

Surfaces with the (111) orientation in the face-centred cubic (fcc) structure were simulated. Slabs of $12 \times 12 \times 100$ supercells (see Fig. 1) with periodic boundary conditions along the x and y directions were used. To check the surface segregation in both reactive and vacuum conditions, one of the two surfaces was exposed to H_2 and the other to vacuum. We fixed the partial pressure of H_2 at 1 atm. We performed MC simulations in the NVT ensemble. The MC moves consisted of surface-surface, surface-bulk, or bulk-bulk swaps of atoms of different species. We performed $3 \cdot 10^6$ swaps in total ($1 \cdot 10^6$ for equilibration and $2 \cdot 10^6$ for sampling) to obtain converged configurations. In order to guide the MC exploration to the

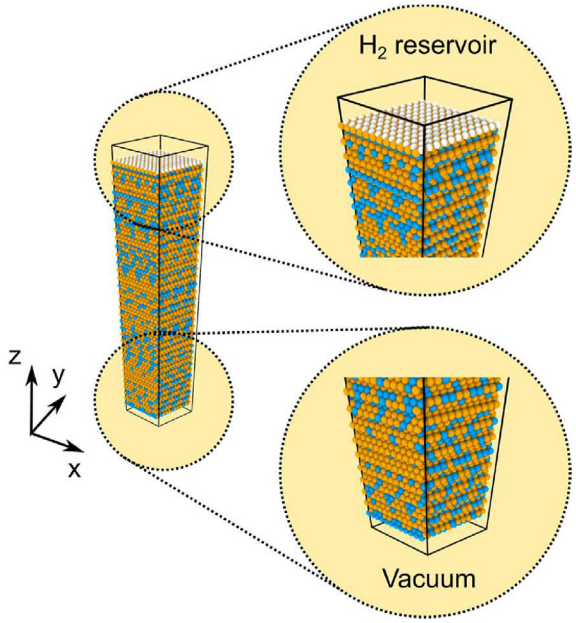

Fig. 1 – The fcc(111) slab used for our Monte Carlo simulations. The top surface is exposed to a H_2 reservoir, the bottom one to vacuum.

global minimum, the system was slowly cooled from 2000 K to T for the first 5% of the simulation. Atomic swaps associated with a total energy change ΔE were accepted according to Metropolis' rule, i.e. with an acceptance probability

$$\min\left[1, \exp\left(\frac{-\Delta E}{k_B T}\right)\right]. \quad (1)$$

For every MC step, we assumed that a H atom can adsorb or desorb from a random position on the surface exposed to hydrogen gas with a probability of 1%, i.e. the coverage of H on the surface was allowed to increase or decrease on average every 100 steps. The probability that an adsorbed H desorbs, or a free site on the surface is populated with H, is

$$\min\left[1, \exp\left(\pm\frac{E_{ads}}{k_B T}\right)\right], \quad (2)$$

where the + sign holds for desorption and the − sign for adsorption, respectively. The details of the calculation of ΔE and E_{ads} are provided in the next subsections.

Energy change of atomic swaps

To evaluate the energy change associated with atomic swaps, we considered a broken-bond model [31], where each atom interacts only with its nearest neighbours and only via pairwise terms. If the binding energy between atoms of type i and j is ε_{ij}, the alloy parameter for $i-j$ is defined as

$$\omega_{ij} = \varepsilon_{ij} - \frac{\varepsilon_{ii} + \varepsilon_{jj}}{2} \quad (3)$$

It can be shown that bulk-bulk swaps of two atoms of type A and B at positions 1 and 2 in a ternary alloy A-B-C change the total energy by

$$\Delta E = (Z_1^A - Z_2^A)(\omega_{AB} + \omega_{AC} - \omega_{BC}) + (Z_1^B - Z_2^B)(-\omega_{AB} + \omega_{AC} - \omega_{BC}), \quad (4)$$

where Z_1^A is the number of A atoms that surround site 1, Z_2^A the number of A atoms that surround site 2, Z_1^B is the number of B atoms that surround site 1 and Z_2^B the number of B atoms that surround site 2. We computed the alloy parameters ω_{ij} with Miedema's model following Ref. [33], which proposes a combination of the geometric Miedema's model by Ouyang et al. [36] and a two-step Miedema's model by Wang et al. [37]. In brief, the general approach for extending the Miedema's model to ternary alloys is by averaging the sub-binary alloys that are contained in the ternary alloy [33,36–42]. Similarly, to bulk-bulk swaps, the energy change associated with surface-surface swaps is

$$\Delta E = (Z_1^A - Z_2^A)(\omega_{AB} + \omega_{AC} - \omega_{BC}) + (Z_1^B - Z_2^B)(-\omega_{AB} + \omega_{AC} - \omega_{BC}) + \Delta E_{ads} \quad (5)$$

where the extra term ΔE_{ads} accounts for the eventual energy change if sites 1 or 2 are adjacent to an adsorbed H atom.

The total energy change related to bulk-surface swaps involves more terms, associated with the change of the overall surface energy of the alloy and the release of the elastic misfit energy [31–33]:

$$\Delta E = (Z_1^A - Z_2^A)(\omega_{AB} + \omega_{AC} - \omega_{BC}) + (Z_1^B - Z_2^B)(-\omega_{AB} + \omega_{AC} - \omega_{BC}) + Z_v(\omega_{BC} - \omega_{AC}) + \gamma_A\sigma_A - \gamma_B\sigma_B + \Delta E_{ads} + \Delta E_{elastic} \quad (6)$$

where $Z_v = 3$ is the number of out-of-plane nearest neighbours for the fcc (111) geometry, γ_A and, γ_B are the surface energies of pure A and B metals and σ_A and σ_B are the unit surface areas of A and B for the fcc (111) surface. The elastic energy $\Delta E_{elastic}$ was evaluated using the geometric model proposed by Ouyang et al. [36]. The equation for the elastic energy as originally introduced in the dilute limit is not symmetric and this results in artificially different values of the elastic energy at equiatomic compositions when the solute and solvent are switched. To solve this issue, we took a weighted average of the elastic energy. This ensured that the detailed balance was preserved, which was necessary for the MC simulations:

$$\Delta E_{elastic} = c_A \cdot \Delta E_{elastic}^{AB} - c_B \cdot \Delta E_{elastic}^{BA} + c_C\left(\Delta E_{elastic}^{CB} - \Delta E_{elastic}^{CA}\right) \quad (7)$$

where c_A, c_B and c_C are the concentrations of elements A, B and C, respectively.

Adsorption energy

The energy change associated to the adsorption of a H atom on a surface site is

$$E_{ads} = E_{ads}^{(0)} - \mu(T) \quad (8)$$

with $E_{ads}^{(0)}$ the adsorption energy of H on the surface at 0 K and $\mu(T)$ the chemical potential of a hydrogen atom at 1 atm. We parametrized $\mu(T)$ from thermochemical tables [43]. When available, $E_{ads}^{(0)}$ was taken from Ref. [23], otherwise we computed it with DFT as

$$E_{ads}^{(0)} = \frac{E_{M+2H} - E_M - E_{H_2}}{2} \quad (9)$$

where E_{M+2H} is the energy of a slab with a H atom adsorbed on both surfaces, E_M the energy associated to the slab in vacuum and E_{H_2} the energy of a hydrogen molecule. We neglected H–H interactions on the surface, since they are only relevant at temperatures below 200 K [44].

Since the H atoms preferentially adsorb on the fcc hollow sites [45], an adsorbed H atom on a fcc site is surrounded by three atoms. For simplicity, we took $E_{ads}^{(0)}$ as the average adsorption energy of the three pure metals surrounding the H atom.

Density functional theory calculations

DFT calculations were performed using the plane-wave projector augmented wave (PAW) method [46,47] as implemented in VASP 5.4 [48–50]. The generalized gradient approximation in the Perdew-Burke-Ernzerhof (PBE) parametrization was used for the exchange-correlation potential [51]. An energy cutoff of 400 eV and a k-mesh density of 0.125 $2\pi/$Å ensured converged energy differences. Smearing of the electronic states was applied with the Methfessel-Paxton function [52] with a width of 0.1 eV. The atomic positions were relaxed until the energy decreased by less than 10^{-4} eV. To calculate $E_{ads}^{(0)}$, the fcc (111) surfaces were modelled as $1 \times 1 \times 7$ slabs with 30 Å of vacuum. This value is large enough to prevent spurious interactions with the periodic images along the z direction.

CALPHAD calculations

The CALPHAD calculations to assess the stability of the fcc phase in our high-throughput search for Pd–Cu–X membranes were performed with the Thermo-Calc 2019b software package [53] using the SSOL2 database.

Model benchmark

Comparison between MC and the LM equation

As a first benchmark, we compared the MC method with the LM equation. Fig. 2 displays the concentrations of Ag and Au in the n-th layers (the first being the surface) as a function of the bulk composition in binary Pd–Ag and Pd–Au alloys. The solid lines refer to the MC results, the black crosses to the LM equation. For these alloys, Ag and Au segregate on the surface and there is also a mild anti-segregation of Ag in the subsurface layer. It can be clearly seen that the difference between MC simulations and the LM equation is small (maximum 5 at. %) for binary alloys and we conclude that for these alloys the effect of short-range order is not relevant.

Contrary to binary systems, the LM equation can lead to quantitatively wrong predictions in ternary alloys. In this case, short-range ordering, co-segregation, site-competition, and blocking mechanisms can have significant effects. These effects are enhanced by mixing elements from opposite ends of the transition metal series, because the mixing energies are higher in magnitude; for instance, Fig. 3 shows the layer-by-layer composition of the alloy $Pd_{50}Cu_{10}La_{40}$ predicted by the MC method (circles) and by the LM equation (crosses). The MC simulations predict that Pd and La segregate at the surface in

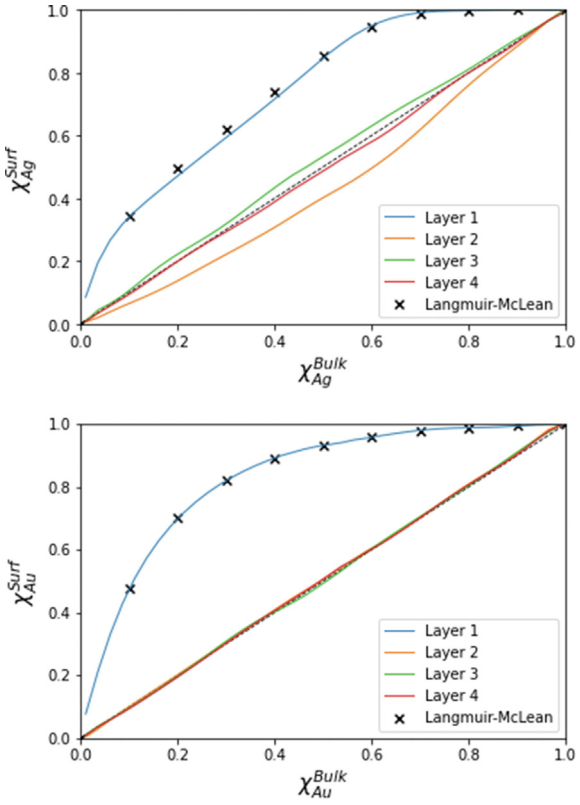

Fig. 2 – Surface segregation of Pd–Ag and Pd–Au in vacuum at 600 K in atomic fractions. The no-segregation line is indicated by the dotted line. Atomic fractions above the dotted line indicate surface segregation of the alloying element (i.e. Ag or Au). The coloured lines are predicted by our model. The crosses indicate predictions of the surface fraction by the LM equation. (a) Pd-Ag. (b) Pd-Au.

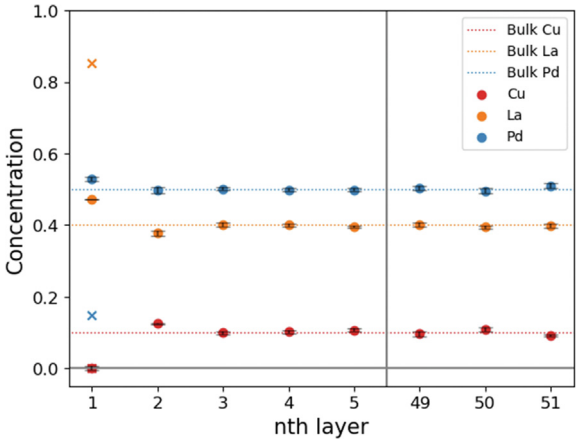

Fig. 3 – Predicted atomic fraction at the surface in $Pd_{50}Cu_{10}La_{40}$ at 600 K in vacuum by the LM equation (crosses) and by MC simulations (circles). Layer 49 to 51 show the bulk composition.

almost equal concentrations, whereas the LM result shows a predominant La segregation. In this case, a difference as high as 41 at. % between the MC simulations and the result from the LM equation is observed for the surface layer. The mixing energies of Pd–La and Cu–La are −0.56 eV and −0.51 eV respectively, thus want to mix, and are roughly 5 times larger than the mixing energy of Pd–Cu. The surface energy and elastic energy in this alloy are small in comparison to the mixing energy and have a negligible effect. La therefore stays in the bulk, in order to maximize the amount of Pd and Cu neighbours and blocking occurs. Therefore, using the LM equation may be inappropriate for certain ternary alloys.

Surface segregation in binary alloys

To test the quantitative predictions of our model, we first compared our results against the available literature for binary Pd–Ag, Pd–Au, and Pd–Cu alloys. Surface segregation predictions of Pd alloys from our model are compared to the literature in Table 1. First of all, our results agree well with the other works using Miedema's model, as we observe a maximum deviation of only of 5 at. %, likely due to small ordering effects as mentioned earlier.

The results from our model agree also well with most of the other instances in the literature in a range of −9 at. % to +12 at. %, with the exception of the Pd-rich Pd–Ag alloys from Refs. [54,55]. However, we note that the experimental results from Ref. [55] show a larger segregation at 920 K than at 720 K, indicating that the sample is not in thermodynamic equilibrium, hence these results may not be trustworthy for a quantitative comparison. Nevertheless, all models and experiments capture qualitatively the Ag segregation in Pd–Ag.

Surface segregation in ternary alloys

The available literature on the segregation tendencies in Pd-based ternary alloys is much scarcer than that for binary alloys. Here we tested our model on Pd–Cu–Au, for which experimental data exist for the whole compositional space, and on $Pd_{61}Cu_{29}Ag_{10}$ and $Pd_{84}Cu_5Mo_{11}$.

Fig. 4 shows the excess surface segregation predicted by our model in the Pd–Cu–Au compositional space at 600 K in vacuum. Blue regions indicate depletion of an element on the surface, whereas red regions indicate enrichment. Our results qualitatively follow the trends reported in Ref. [60], in particular: i) the strong depletion of Pd and enrichment of Cu and Au for Pd-rich compositions; ii) the enrichment of Au and depletion of Pd for Au-rich compositions; and iii) the "island" of strong Cu enrichment and Pd depletion around $Pd_{60}Cu_{40}$. We point out however two differences: i) the absolute values of the enrichment/depletion from our work (−0.90 to +0.80) are much larger than those observed experimentally (−0.35 to +0.35); ii) for Cu-rich compositions, we predict a small depletion of Au whereas Ref. [60] reports a small enrichment. The first discrepancy may be due to kinetic limitations in the experiments: by comparing the experimental data at 500 K

Table 1 – Surface segregation from literature compared to the predictions from this work.

Ref.	Method	T (K)	Composition bulk (at. %)	Surface composition literature (at. %)	Surface composition this work (at. %)
[55]	STM	720	$Pd_{67}Ag_{33}$	$Pd_{11}Ag_{89}$	$Pd_{38}Ag_{62}$
		920	$Pd_{67}Ag_{33}$	Pd_5Ag_{95}	$Pd_{41}Ag_{59}$
[32]	Miedema + LM	600	$Pd_{75}Ag_{25}$	$Pd_{48}Ag_{52}$	$Pd_{49}Ag_{51}$
[54]	DFT+ Mean field[a]	600	$Pd_{70}Ag_{30}$	$Pd_{12}Ag_{88}$	$Pd_{41}Ag_{59}$
		900	$Pd_{70}Ag_{30}$	$Pd_{20}Ag_{80}$	$Pd_{45}Ag_{55}$
		600	$Pd_{50}Ag_{50}$	$Pd_{10}Ag_{90}$	$Pd_{18}Ag_{82}$
		900	$Pd_{50}Ag_{50}$	$Pd_{15}Ag_{85}$	$Pd_{19}Ag_{81}$
		900	$Pd_{30}Ag_{70}$	Pd_3Ag_{97}	Pd_2Ag_{98}
[56]	DFT+ LM	0	$Pd_{50}Ag_{50}$	Pd_0Ag_{100}	Pd_0Ag_{100}
		300	$Pd_{50}Ag_{50}$	Pd_8Ag_{92}	$Pd_{10}Ag_{90}$
		600	$Pd_{50}Ag_{50}$	$Pd_{19}Ag_{81}$	$Pd_{18}Ag_{82}$
		900	$Pd_{50}Ag_{50}$	$Pd_{25}Ag_{75}$	$Pd_{19}Ag_{81}$
		1200	$Pd_{50}Ag_{50}$	$Pd_{28}Ag_{72}$	$Pd_{27}Ag_{73}$
[57]	LEIS, XPS	800	$Pd_{50}Au_{50}$	$Pd_{18}Au_{82}$	$Pd_{12}Au_{88}$
			$Pd_{25}Au_{75}$	Pd_6Au_{94}	Pd_4Au_{96}
			$Pd_{75}Au_{25}$	$Pd_{35}Au_{65}$	$Pd_{34}Au_{66}$
[58]	LEIS	875	$Pd_{40}Au_{60}$	Pd_5Au_{95}	Pd_9Au_{91}
			$Pd_{60}Au_{40}$	$Pd_{30}Au_{70}$	$Pd_{21}Au_{79}$
[32]	Miedema + LM	600	$Pd_{75}Au_{25}$	$Pd_{29}Au_{71}$	$Pd_{24}Au_{76}$
[34]	Miedema + LM	800	$Pd_{50}Au_{50}$	$Pd_{20}Au_{80}$	$Pd_{12}Au_{88}$
[34]	LEIS, XPS	1000	$Pd_{60}Cu_{40}$	$Pd_{50}Cu_{50}$	$Pd_{49}Cu_{51}$
[59]	LEIS, XPS	700	$Pd_{48}Cu_{52}$	$Pd_{20}Cu_{80}$	$Pd_{32}Cu_{68}$
		900	$Pd_{48}Cu_{52}$	$Pd_{24}Cu_{76}$	$Pd_{31}Cu_{69}$
		700	$Pd_{40}Cu_{60}$	$Pd_{17}Cu_{83}$	$Pd_{20}Cu_{80}$
		900	$Pd_{40}Cu_{60}$	$Pd_{19}Cu_{81}$	$Pd_{19}Cu_{81}$
[32]	Miedema + LM	600	$Pd_{75}Cu_{25}$	$Pd_{74}Cu_{26}$	$Pd_{69}Cu_{31}$

[a] Modified mean field model that includes subsurface layers.

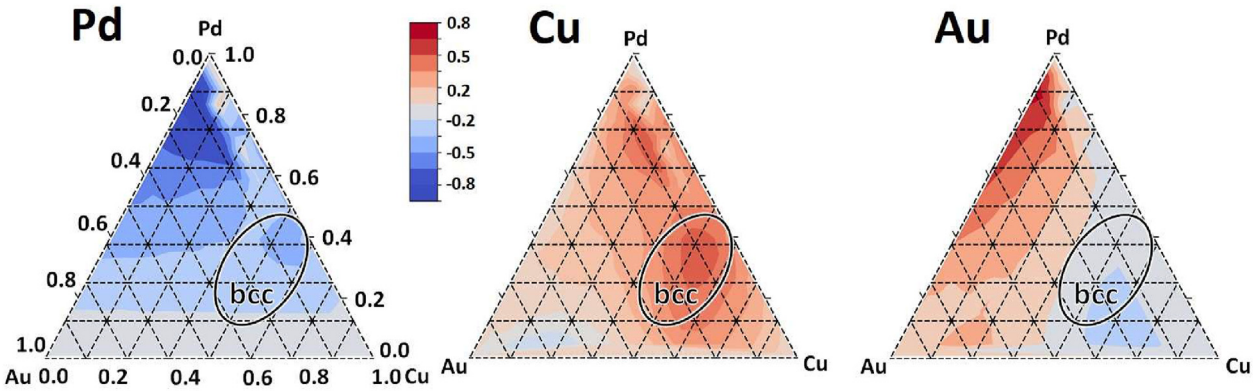

Fig. 4 – Predicted excess atomic fraction at the surface in Pd–Cu–Au at 600 K. Blue regions indicate depletion of the element from the surface, whereas red regions show enrichment of the element on the surface. A region where the body-centred cubic (bcc) phase is stable is roughly outlined. (For interpretation of the references to colour in this figure legend, the reader is referred to the Web version of this article.)

and 600 K in Ref. [60], we notice that the segregation seems to be more pronounced at high temperature, which signals that the alloy is in a metastable state at 500 K, and presumably also at 600 K. We believe that annealing for a longer time or at a higher temperature may lead to segregation profiles closer to our data. The second discrepancy may be due to our simplified treatment of the elastic energy: Cu and Au have similar surface energies; hence the elastic term has a decisive role in determining which element segregates. Another factor that may explain this difference is that the body-centred cubic (bcc) phase is known to be stable for some Cu-rich compositions (approximately outlined in Fig. 4) [61], whereas we only considered the fcc phase. Table 2 compares the composition of the surface of $Pd_{61}Cu_{29}Ag_{10}$ at 1000 K predicted by our model to the experimental and theoretical results from Ref. [33]. In vacuum, both our model and that of Ref. [33], based on the LM equation and Miedema's model, predict that Cu and Ag are enriched and Pd is depleted from the surface, in qualitative agreement with the experiments. In a H_2 atmosphere, it is found experimentally that Ag and Cu are depleted, in qualitative agreement with the predictions of both models. Quantitatively, like for Pd–Cu–Au, theoretical models tend to overestimate segregation when compared to experimental measurements.

Similarly to the model in Ref. [33], we also observe a complete depletion of Cu and Mo from the surface of $Pd_{84}Cu_5Mo_{11}$ at 1000 K, both in vacuum and in a H_2 atmosphere.

Accuracy and limitations of our model

Despite its simplicity, our model accurately predicts the segregation trends in binary and ternary alloys. For systems that can be well approximated as ideal solid solutions, our model shows similar results as the LM equation. However, for ternary or more complex systems when long- or short-range ordering, co-segregation, site-competition, or blocking may play a significant role, our model performs better than other state-of-the-art empirical methods based on the LM equation. Eventual quantitative inaccuracies of the segregation predictions are ascribed to (i) the approximations of the calculation of the binding and segregation energies with Miedema's model, for which Ref. [37] estimated a mean absolute error of roughly 0.05 eV with respect to calorimetry experiments, and (ii) to our simplifying assumption that the interactions between the atoms are only pairwise and short-ranged. We also should emphasize that our model may give biased predictions for elements with similar surface energy but different atomic volumes (like Cu and Au), due to the simplistic treatment of the elastic energy. Moreover, caution is advised when comparing to experimental data, for which full thermodynamic equilibrium may not be reached.

Nevertheless, we believe that our model is very well suited to perform high-throughput searches to design surface and near-surface alloys with tailored properties, as showcased in the next Section.

Table 2 – Reported segregation of Pd–Ag–Cu from Zhao et al. [33] of the surface layer measured with low-energy ion scattering spectroscopy and calculated using Miedema's model in combination with the LM equation in vacuum and with a monolayer coverage. This is compared to the computational model from this work in vacuum and a 2/3 monolayer coverage of H.

Condition	Experimental. (at. %)		Calculated Zhao*et al.* (at. %)		Calculated this work (at. %)	
	Cu	Ag	Cu	Ag	Cu	Ag
Before segregation	29.4	10.4	30.0	10.0	29.4	10.4
1000 K in vacuum	45.1	15.3	54.4	16.5	67.3	25.0
1000 K in 1 bar H_2	23.2	7.6	29.9	3.9	9.0	0.0

Design of novel Pd–Cu–X membranes

The model from this work was applied in a general workflow to design new Pd-based H_2 separation membranes. The target properties that needed to be optimized were: permeability of H, cost of the component elements, thermodynamic stability, and resistance to poisoning.

We started from binary Pd–Cu membranes, that were shown to possess high poisoning resistance at 670 K and 770 K at a composition of $Pd_{70}Cu_{30}$ [62] and looked for candidate alloying elements X to form Pd–Cu–X membranes such that: i) X increases the lattice parameter thereby improving the H diffusivity and X has high solubility, thereby increasing permeability [63]; ii) X decreases the overall cost of the alloy; iii) the resulting alloy is a single-phase solid solution in the fcc phase; iv) the addition of X leads to a surface composition close to $Pd_{70}Cu_{30}$, which is needed for poisoning resistance.

Our workflow is schematically displayed in Fig. 5: we first considered all the transition metals (Input), then we selected all the elements with a larger lattice parameter and solubility to H than Pd and Cu and which are not more expensive than Pd (Wishes). For each of the resulting Pd–Cu–X alloys, we performed CALPHAD calculations to assess the regions of the phase diagram where a single fcc phase is stable at a temperature of 1000 K, a typical annealing temperature for processing (Stability). Finally, we used our model to determine the alloy composition so that a $Pd_{70}Cu_{30}$ surface alloy is stable on the surface exposed to H_2, that is, the alloying element X segregates in the bulk and it does not interfere with the dissociation and adsorption of hydrogen (Segregation).

From this selection process, Zr is found to be the most promising candidate. In particular, as shown in Fig. 6, our model predicts that for a bulk composition of $Pd_{48}Cu_{40}Zr_{12}$ the composition of the surface exposed to H_2 (100th layer) is close to the target $Pd_{70}Cu_{30}$ at 700 K. A membrane with composition $Pd_{48}Cu_{40}Zr_{12}$ would increase the H permeability and cut the cost when compared to Pd–Cu membranes, due to the partial substitution of Pd for Zr. For this composition, the fcc phase is stable at $T > 1000$ K. From our CALPHAD simulations, for $T < 1000$ K, a small fraction of the hexagonal close-packed (hcp) phase may precipitate, but we expect this precipitation to be kinetically hindered. According to the MC simulations, it maintains the nominal composition in the bulk and shows the favourable $Pd_{70}Cu_{30}$ composition on the H_2 exposed surface, which prevents poisoning.

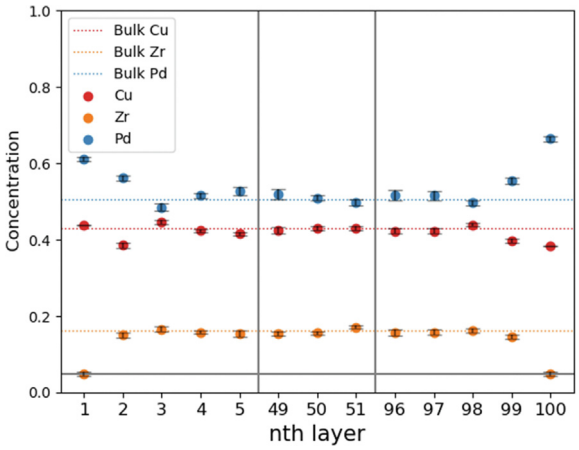

Fig. 6 – Average concentration of the component elements of $Pd_{48}Cu_{40}Zr_{12}$ at 700 K for the first five subsurface layers (1–5 and 96–100) and for three bulk layers (49–51). Layer 1 is exposed to vacuum, layer 100 is exposed to H_2. The horizontal lines indicate the nominal bulk composition.

Fig. 5 – Approach to tailor the surface composition of a ternary alloy.

We validated the segregation of Zr to the bulk with DFT. To this end, we randomly extracted five snapshots from a MC simulation on a smaller $3 \times 3 \times 7$ slab at 700 K, swapped the element Zr from a random position in the bulk to a random position on each surface for 15 different positions, and then calculated the energy difference associated with each swap. We thus computed a total of 75 energy differences for the surface exposed to H_2 and 75 for that exposed to vacuum. Forcing Zr to the surface is indeed unfavourable: the energy increases by 0.25 ± 0.08 eV when Zr is put on the surface exposed to H_2 and by 0.58 ± 0.10 eV when Zr is put on the surface exposed to vacuum. This confirms the prediction of our model that alloying with Zr improves the bulk properties of Pd–Cu membranes without altering the favourable surface properties, i.e. high H_2 dissociation rate and low poisoning.

Conclusions

Surface segregation is of great importance as catalytic reactions are mostly determined by the surface layer. In this work, we developed a model to predict the equilibrium composition of the surface and subsurface layers of arbitrary ternary alloys. Our model is based on Monte Carlo simulations combined with semi-empirical thermodynamic methods. We benchmarked the results from our model against the available literature on Pd-based alloys and found that it predicts similar segregation profiles as other state-of-the-art methods for ideal solid solutions. However, in contrast to other methods, it can take into account short-range ordering, co-segregation, site-competition, and blocking mechanisms for non-ideal systems. We employed our model to design novel hydrogen separation membranes with improved properties and we verified our predictions with Density Functional Theory. We propose the $Pd_{48}Cu_{40}Zr_{12}$ alloy for more efficient, more stable and less expensive hydrogen separation membranes. A membrane with a similar composition was fabricated by Nayebossadri et al. and displayed higher stability and improved tolerance against sulphur poisoning compared to Pd–Cu membranes [64].

Data availability

The code used for the Monte Carlo simulations can be found here.

Declaration of competing interest

The authors declare that they have no known competing financial interests or personal relationships that could have appeared to influence the work reported in this paper.

Acknowledgements

A.F. was supported by the Nederlandse Organisatie voor Wetenschappelijk Onderzoek (NWO) [VIDI Grant No. 15707]. The authors thank Marcel Sluiter and Fritz Körmann for helpful discussions and suggestions.

REFERENCES

[1] Dunn S. Hydrogen futures: toward a sustainable energy system. Int J Hydrogen Energy 2002;27:235–64. https://doi.org/10.1016/S0360-3199(01) 00131-8.
[2] Kim T, Song Y, Kang J, Kim SK, Kim S. A review of recent advances in hydrogen purification for selective removal of oxygen: deoxo catalysts and reactor systems. Int J Hydrogen Energy 2022;47:24817–34. https://doi.org/10.1016/j.ijhydene.2022.05.221.
[3] Bernardo G, Araújo T, da Silva Lopes T, Sousa J, Mendes A. Recent advances in membrane technologies for hydrogen purification. Int J Hydrogen Energy 2020;45:7313–38. https://doi.org/10.1016/j.ijhydene.2019.06.162.
[4] Fraile D, Lanoix J-C, Maio P, Rangele A, Torres A. Overview of the market segmentation for hydrogen across potential customer groups, based on key application areas. Technical Report; 2015.
[5] ISO, INTERNATIONAL. STANDARD Hydrogen fuel — product fuel cell applications for road vehicles. Technical Report; 2012.
[6] Timofeev N, Berseneva F, Makarov V. New palladium-based membrane alloys for separation of gas mixtures to generate ultrapure hydrogen. Int J Hydrogen Energy 1994;19:895–8. https://doi.org/10.1016/0360-3199(94)90042-6.
[7] Tosti S, Basile A, Bettinali L, Borgognoni F, Gallucci F, Rizzello C. Design and process study of Pd membrane reactors. Int J Hydrogen Energy 2008;33:5098–105. https://doi.org/10.1016/j.ijhydene.2008.05.031.
[8] Al-Mufachi N, Rees N, Steinberger-Wilkens R. Hydrogen selective membranes: a review of palladium-based dense metal membranes. Renew Sustain Energy Rev 2015;47:540–51. https://doi.org/10.1016/j. rser.2015.03.026.
[9] Tarditi AM, Cornaglia LM. Novel PdAgCu ternary alloy as promising materials for hydrogen separation membranes: synthesis and characterization. Surf Sci 2011;605:62–71. https://doi.org/10.1016/j.susc.2010.10.001.
[10] Adams BD, Chen A. The role of palladium in a hydrogen economy. Mater Today 2011;14:282–9. https://doi.org/10.1016/S1369-7021(11)70143-2.
[11] Ockwig NW, Nenoff TM. Membranes for hydrogen separation. Chem Rev 2007;107:4078–110. https://doi.org/10.1021/cr0501792.
[12] Helmi A, Gallucci F, Van Sint Annaland M. Resource scarcity in palladium membrane applications for carbon capture in integrated gasification combined cycle units. Int J Hydrogen Energy 2014;39:10498–506. https://doi.org/10.1016/j.ijhydene.2014.05.009.
[13] Berseneva F, Timofeev N, Zakharov A. Alloys of palladium with metals of the platinum group as hydrogen-permeable membrane components at high temperatures of gas separation. Int J Hydrogen Energy 1993;18:15–8. https://doi.org/10.1016/0360-3199(93)90097-T.
[14] Yun S, Ted Oyama S. Correlations in palladium membranes for hydrogen separation: a review. J Membr Sci 2011;375:28–45. https://doi.org/10.1016/j.memsci.2011.03.057.
[15] Lewis FA. Hydrogen in palladium and palladium alloys. Int J Hydrogen Energy 1996;21:461–4. https://doi.org/10.1016/0360-3199(95)00126-3.
[16] Ali JK, Newson EJ, Rippin DW. Deactivation and regeneration of PdAg membranes for dehydrogenation reactions. J Membr

Sci 1994;89:171–84. https://doi.org/10.1016/0376-7388(93)E0219-A.
[17] Hatlevik Ø, Gade SK, Keeling MK, Thoen PM, Davidson AP, Way JD. Palladium and palladium alloy membranes for hydrogen separation and production: history, fabrication strategies, and current performance. Separ Purif Technol 2010;73:59–64. https://doi.org/10.1016/j.seppur.2009.10.020.
[18] Sakamoto Y, Chen FL, Furukawa M, Noguchi M. Permeability and diffusivity of hydrogen in palladium-rich Pd-Y(Gd)-Ag ternary alloys. J Alloys Compd 1992;185:191–205. https://doi.org/10.1016/0925-8388(92)90468-O.
[19] Pomerantz N, Ma YH. Effect of H_2S on the performance and long-term stability of Pd/Cu membranes. Ind Eng Chem Res 2009;48:4030–9. https://doi.org/10.1021/ie801947a.
[20] Chen CH, Ma YH. The effect of H_2S on the performance of Pd and Pd/Au composite membrane. J Membr Sci 2010;362:535–44. https://doi.org/10.1016/j.memsci.2010.07.002.
[21] Mundschau MV, Xie X, Evenson IV CR, Sammells AF. Dense inorganic membranes for production of hydrogen from methane and coal with carbon dioxide sequestration. Catal Today 2006;118:12–23. https://doi.org/10.1016/j.cattod.2006.01.042.
[22] Jia H, Wu P, Zeng G, Salas-Colera E, Serrano A, Castro GR, Xu H, Sun C, Goldbach A. High-temperature stability of Pd alloy membranes containing Cu and Au. J Membr Sci 2017;544:151–60. https://doi.org/10.1016/j.memsci.2017.09.012.
[23] Tománek D, Mukherjee S, Kumar V, Bennemann KH. Calculation of chemisorption and absorption induced surface segregation. Surf Sci 1982;114:11–22. https://doi.org/10.1016/0039-6028(82)90452-6.
[24] Bosko ML, Dalla Fontana A, Tarditi A, Cornaglia L. Advances in hydrogen selective membranes based on palladium ternary alloys. Int J Hydrogen Energy 2021;46:15572–94. https://doi.org/10.1016/j.ijhydene.2021.02.082.
[25] Lai T, Lind ML. Heat treatment driven surface segregation in pd77ag23 membranes and the effect on hydrogen permeability. Int J Hydrogen Energy 2015;40:373–82. https://doi.org/10.1016/j. ijhydene.2014.11.017.
[26] McLean D. Grain boundaries in metals. Oxford: Clarendon Press; 1957.
[27] Luyten J, Creemers C. Surface segregation in ternary Pt-Pd-Rh alloys studied with Monte Carlo simulations and the modified embedded atom method. Surf Sci 2008;602:2491–5. https://doi.org/10.1016/j.susc.2008.05.024.
[28] Daw MS, Baskes MI. Embedded-atom method: derivation and application to impurities, surfaces, and other defects in metals. Phys Rev B 1984;29:6443. https://doi.org/10.1103/PhysRevB.29.6443.
[29] De Boer FR, Mattens W, Boom R, Miedema A, Niessen A. Cohesion in metals. Transition metal alloys. 1988.
[30] Sundman B, Jansson B, Andersson JO. The Thermo-Calc databank system. Calphad 1985;9:153–90. https://doi.org/10.1016/0364-5916(85).90021-5.
[31] Wynblatt P, Ku RC. Surface energy and solute strain energy effects in surface segregation. Surf Sci 1977;65:511–31. https://doi.org/10.1016/0039-6028(77)90462-9.
[32] Zhao M, Sloof WG, Böttger AJ. Modelling of surface segregation for palladium alloys in vacuum and gas environments. Int J Hydrogen Energy 2018;43:2212–23. https://doi.org/10.1016/j.ijhydene.2017.12.039.
[33] Zhao M, Brouwer JC, Sloof WG, Böttger AJ. Surface segregation of ternary alloys: effect of the interaction between solute elements. Adv Mater Interfac 2020;7:1–9. https://doi.org/10.1002/admi.201901784.
[34] Zhao M, Brouwer JC, Sloof WG, Böttger AJ. Surface segregation of Pd–Cu alloy in various gas atmospheres. Int J Hydrogen Energy 2020;45:21567–72. https://doi.org/10.1016/j.ijhydene.2020.05.268.
[35] Herbst JF. On extending Miedema's model to predict hydrogen content in binary and ternary hydrides. J Alloys Compd 2002;337:99–107. https://doi.org/10.1016/S0925-8388(01)01939-9.
[36] Ouyang Y, Zhong X, Du Y, Jin Z, He Y, Yuan Z. Formation enthalpies of Fe-Al-RE ternary alloys calculated with a geometric model and Miedema's theory. J Alloys Compd 2006;416:148–54. https://doi.org/10.1016/j.jallcom.2005.08.055.
[37] Wang WC, Li JH, Yan HF, Liu BX. A thermodynamic model proposed for calculating the standard formation enthalpies of ternary alloy systems. Scripta Mater 2007;56:975–8. https://doi.org/10.1016/j.scriptamat.2007.01.044.
[38] Gonçalves AP, Almeida M. Extended Miedema model: predicting the formation enthalpies of intermetallic phases with more than two elements. Phys B Condens Matter 1996;228:289–94. https://doi.org/10.1016/S0921-4526(96)00480-00482.
[39] Zhang B, Jesser WA. Formation energy of ternary alloy systems calculated by Miedema model. Phys B Condens Matter 2002;315:123–32. https://doi.org/10.1016/S0921-4526(01)00964-4.
[40] Ray P, Akinc M. Estimation of formation enthalpies using an extended Miedema approach. In: 22nd Annual Conference on Fossil Energy Materials; 2008. URL: http://seca.doe.gov/publications/proceedings/08/fem/manuscripts/Kramer.pdf.
[41] Sadeghi E, Karimzadeh F, Abbasi MH. Thermodynamic analysis of Ti-Al-C intermetallics formation by mechanical alloying. J Alloys Compd 2013;576:317–23. https://doi.org/10.1016/j.jallcom.2013.05.196.
[42] Mousavi MS, Abbasi R, Kashani-Bozorg SF. A thermodynamic approach to predict formation enthalpies of ternary systems based on Miedema's model. Metall Mater Trans A 2016;47:3761–70. https://doi.org/10.1007/s11661-016-3533-4.
[43] Chase M, Davies C, Downey D, Frurip Jr JR, McDonald R, Syverud A. Nist-janaf thermochemical tables. URL: https://jana.nist.gofv/pdf/JANAF-FourthEd-1998-Hydrogen.pdf; 1998.
[44] Montoya A, Schlunke A, Haynes BS. Reaction of hydrogen with Ag(111): binding states, minimum energy paths, and kinetics. J Phys Chem B 2006;110:17145–54. https://doi.org/10.1021/jp062725g.
[45] Watson GW, Wells RP, Willock DJ, Hutchings GJ. A comparison of the adsorption and diffusion of hydrogen on the 111 surfaces of Ni, Pd, and Pt from density functional theory calculations. J Phys Chem B 2002;105:4889–94. https://doi.org/10.1021/jp002864c.
[46] Blöchl PE. Projector augmented-wave method. Phys Rev B 1994;50:17953. https://doi.org/10.1103/PhysRevB.50.17953.
[47] Kresse G, Joubert D. From ultrasoft pseudopotentials to the projector augmented-wave method. Phys Rev B 1999;59:1758. https://doi.org/10.1103/PhysRevB.59.1758.
[48] Kresse G, Hafner J. Ab initio molecular dynamics for liquid metals. Phys Rev B 1993;47:558. https://doi.org/10.1103/physrevb.47.558.
[49] Kresse G, Furthmüller J. Efficiency of ab-initio total energy calculations for metals and semiconductors using a plane-wave basis set. Comput Mater Sci 1996;6:15–50. https://doi.org/10.1016/0927-0256(96)00008-0.
[50] Kresse G, Furthmüller J. Efficient iterative schemes for ab initio totalenergy calculations using a plane-wave basis set. Phys Rev B 1996;54:11169. https://doi.org/10.1103/PhysRevB.54.11169.
[51] Perdew JP, Burke K, Ernzerhof M. Generalized gradient approximation made simple. Phys Rev Lett 1996;77:3865–8. https://doi.org/10.1103/PhysRevLett.77.3865.

[52] Methfessel M, Paxton A. High-precision sampling for Brillouin-zone integration in metals. Phys Rev B 1989;40:3616. https://doi.org/10.1103/.PhysRevB.40.3616.
[53] Andersson J-O, Helander T, Höglund L, Shi P, Sundman B. Thermocalc & dictra, computational tools for materials science. Calphad 2002;26:273–312. https://doi.org/10.1016/S0364-5916(02) 00037-8.
[54] Ropo M, Kokko K, Vitos L, Kollár J, Johansson B. The chemical potential in surface segregation calculations: AgPd alloys. Surf Sci 2006;600:904–13. https://doi.org/10.1016/j.susc.2005.12.023.
[55] Wouda PT, Schmid M, Nieuwenhuys BE, Varga P. STM study of the (111) and (100) surfaces of PdAg. Surf Sci 1998;417:292–300. https://doi.org/10.1016/S0039-6028(98)00673-6.
[56] Ropo M, Kokko K, Vitos L, Kollár J. Segregation at the PdAg(111) surface: electronic structure calculations. Phys Rev B 2005;71:1–6. https://doi.org/10.1103/PhysRevB.71.045411.
[57] Yi CW, Luo K, Wei T, Goodman DW. The composition and structure of Pd - Au surfaces. J Phys Chem B 2005;109:18535–40. https://doi.org/10.1021/jp053515r.
[58] Swartzfager DG, Ziemecki SB, Kelley MJ. Differential sputtering and surface segregation: the role of enhanced diffusion. J Vac Sci Technol 1981;19:185–91. https://doi.org/10.1116/1.571102.
[59] Priyadarshini D, Kondratyuk P, Picard YN, Morreale BD, Gellman AJ, Miller JB. High-throughput characterization of surface segregation in Cu_xPd_{1-x} alloys. J Phys Chem C 2011;115:10155–63. https://doi.org/10.1021/jp201793d.
[60] Yin C, Guo Z, Gellman AJ. Surface segregation across ternary alloy composition space: $Cu_xAu_yPd_{1-x-y}$. J Phys Chem C 2020;124:10605–14. https://doi.org/10.1021/acs.jpcc.0c02058.
[61] Nayebossadri S, Speight J, Book D. Effects of low Ag additions on the hydrogen permeability of Pd-Cu-Ag hydrogen separation membranes. J Membr Sci 2014;451:216–25. https://doi.org/10.1016/j.memsci.2013.10.002.
[62] Peters TA, Kaleta T, Stange M, Bredesen R. Hydrogen transport through a selection of thin Pd-alloy membranes: membrane stability, H_2S inhibition, and flux recovery in hydrogen and simulated WGS mixtures. Catal Today 2012;193:8–19. https://doi.org/10.1016/j.cattod.2011.12.028.
[63] Sakamoto Y, Baba K. The effect of alloying of palladium on the hydrogen-palladium miscibility gap. Zeitschrift fur Physikalische Chemie 1988;158:223–35. https://doi.org/10.1524/zpch.1988.158.Part_2.223.
[64] Nayebossadri S, Speight JD, Book D. Novel Pd–Cu–Zr hydrogen separation membrane with a high tolerance to sulphur poisoning. Chem Commun 2015;51:15842–5. https://doi.org/10.1039/c5cc04327a.